JACS
JOURNAL OF THE AMERICAN CHEMICAL SOCIETY

Communication

pubs.acs.org/JACS

Nano-Chemical Infrared Imaging of Membrane Proteins in Lipid Bilayers

Samuel Berweger,[†,⊥] Duc M. Nguyen,[‡] Eric A. Muller,[†,⊥] Hans A. Bechtel,[∥] Thomas T. Perkins,[§,⊥] and Markus B. Raschke*[,†,⊥]

[†]Department of Physics and Department of Chemistry, [‡]Department of Chemical and Biological Engineering, and [§]Department of Molecular, Cellular, and Developmental Biology, University of Colorado, Boulder, Colorado, 80309, United States

[⊥]JILA, National Institute of Standards and Technology, and University of Colorado, Boulder, Colorado 80309, United States

[∥]Advanced Light Source Division, Lawrence Berkeley National Laboratory, Berkeley, California 94720, United States

Supporting Information

ABSTRACT: The spectroscopic characterization of biomolecular structures requires nanometer spatial resolution and chemical specificity. We perform full spatio-spectral imaging of dried purple membrane patches purified from *Halobacterium salinarum* with infrared vibrational scattering-type scanning near-field optical microscopy (s-SNOM). Using near-field spectral phase contrast based on the Amide I resonance of the protein backbone, we identify the protein distribution with 20 nm spatial resolution and few-protein sensitivity. This demonstrates the general applicability of s-SNOM vibrational nanospectroscopy, with potential extension to a wide range of biomolecular systems.

The multiple functions of a cell emerge from the organization and complex interplay of different biomolecules and subcellular organelles on nanometer length scales. In particular, the structure of the cellular plasma membrane is critical to biological systems. While serving as a largely impenetrable barrier, the embedded proteins perform crucial functions for metabolism, signaling, and control of membrane potential. Hence, understanding the spatial distribution and ordering of membrane proteins has been of great interest.[1] This highlights the general desire to perform ultrahigh spatial resolution imaging combined with optical spectroscopic identification of the chemical identity of cellular constituents.

Photoactivated localization microscopy (PALM),[2] stochastic optical reconstruction microscopy (STORM),[3] and stimulated emission depletion microscopy (STED)[4] have been developed to provide nanometer-scale subdiffraction limit imaging. However, chemical specificity can only be obtained though the selective labeling of the species of interest.

In contrast, apertureless near-field microscopy[5] directly provides the desired nanometer spatial resolution. Moreover it can be combined with label-free vibrational spectroscopies to yield chemical specificity. In such measurements, a sharp scanning probe tip acts as an optical antenna that spatially confines the incident far-field light to dimensions given by the nanoscale tip apex while simultaneously enhancing emission.[6]

Chemically specific nanoscale imaging of biological materials has recently been achieved in tip-enhanced Raman scattering (TERS).[7,8] However, due to the small Raman cross sections of many characteristic biomolecular systems, routine nano-Raman spectroscopy of biological samples is still challenging.

A promising alternative is infrared vibrational scattering-type scanning near-field optical microscopy[9,10] (IR s-SNOM). s-SNOM is based on elastic light scattering, benefits from large molecular bond polarizabilities and yields nanometer spatial resolution. The recent demonstration of its sensitivity to as few as 100 vibrational oscillators or functional groups suggests the feasibility of detecting even single biological macromolecules.[11]

The amide modes associated with the protein peptide bonds are particularly important biomolecular vibrational resonances. They are only weakly Raman active but strongly IR active and, hence, particularly well suited for IR s-SNOM. The amide modes serve as sensitive reporters of protein structure and environment in a variety of spectroscopic techniques including FTIR correlation,[12] ultrafast pump−probe,[13] and nonlinear multidimensional spectroscopies.[14,15]

In this work, we directly identify the distribution and density of the membrane protein bacteriorhodopsin (bR) in dried purple membrane patches purified from *Halobacterium salinarum* by nanoimaging with chemically sensitive label-free spectroscopic IR s-SNOM. We demonstrate spatio-spectral imaging with 20 nm spatial resolution based on the Amide I vibrational mode of bR. Our high contrast obtained suggests a sensitivity sufficient to detect single bR trimers, which opens up the possibility for label-free and chemically specific single biomolecule spectroscopy.

A schematic of the interferometric s-SNOM setup is shown in Figure 1a. A continuous-wave quantum cascade laser (QCL, Daylight Solutions Inc.) provides IR radiation tunable across $\overline{\nu}$ = 1570 − 1720 cm^{-1} with a bandwidth <1 cm^{-1}, covering the Amide I mode. As established in most s-SNOM implementations,[16] we focus the beam in one arm of the Michelson interferometer with an off-axis parabolic mirror (NA = 0.35, P < 10 mW) onto the apex of the tip of an atomic force microscope (AFM, Anasys Instruments). We use Pt-coated cantilevers (Arrow NCPt, NanoWorld AG) with tip apex radius of ∼20 nm operating in tapping mode with frequency ω_t ∼ 250 kHz. The tip-scattered IR radiation is recombined with the reference field for interferometric heterodyne amplification and detection with a

Received: October 1, 2013
Published: November 19, 2013

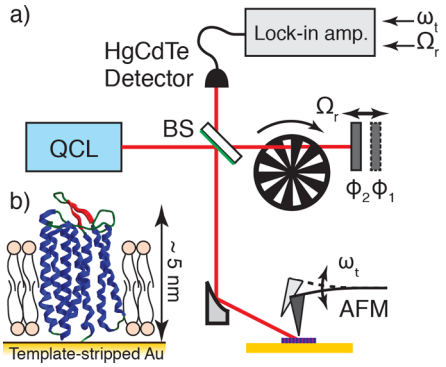

Figure 1. Schematic of the interferometric s-SNOM setup for IR-vibrational nanoimaging of the purple membrane (a). Nanoscale spectroscopic contrast is obtained by tuning the QCL over the Amide I resonance of the peptide bond. Illustration of the membrane protein bR in the lipid bilayer supported on a template-stripped gold substrate (b).

HgCdTe detector (Kolmar Technologies, KLD-0.25-J1−3/11/DC). In order to isolate the near-field signal,[17] we combine several modulation schemes (see Supporting Information) that provide the background-free near-field amplitude |A| and phase ϕ,[18,19] which relate to the complex-valued dielectric function of the Amide I resonance, as discussed below. We acquire raster-scanned s-SNOM images with a lock-in time constant of 10 ms/pixel that yields good near-field signal contrast and avoids sample drift issues.

Purple membrane has been characterized extensively and is simple to prepare in micrometer-scale patches on surfaces. As illustrated in Figure 1b, purple membrane consists of a lipid bilayer with the membrane protein bR, leading to a slight (∼1−2 nm) increased thickness in the protein-rich regions. The bR self-assembles to form trimer subunits that further crystallize into a hexagonal close-packed structure that can be resolved with subnanometer resolution on atomically flat mica.[20,21] Using a commercial AFM (Asylum Instruments, Cypher), we image such hexagonal packing[22] when using standard deposition techniques (Figure S1).[20,21] However, in order to improve the s-SNOM signal level via enhanced tip−sample polarization,[23] we use template-stripped Au as a substrate. The RMS roughness of $\lesssim$0.4 nm of our Au surface precluded imaging the bR lattice, as expected. We perform the s-SNOM studies at room temperature in air and find the samples to be stable with highly reproducible results and no evident deterioration over the period of a month.

In order to identify purple membrane patches for a detailed nanospectroscopic study, we first perform concurrent large area survey s-SNOM and AFM scans of the sample over regions up to 50 mm in size. Figure 2a shows a 20 × 8 μm topographic image of the purple membrane sample exhibiting randomly dispersed irregularly shaped membrane patches. Patch height was ∼5 nm, consistent with a single membrane bilayer.

The simultaneously recorded s-SNOM signal provides corresponding all-optical nanometer-scale resolution images (Figure 2b−d). The near-field amplitude |A| exhibits contrast between the Au substrate and purple membrane patches (Figure 2b). Contrast in the amplitude of the tip-scattered light arises from a reduced optical polarizability of the membrane relative to the gold substrate. The corresponding near-field phase ϕ image exhibits stronger and more specific vibrational contrast under resonant excitation of the Amide I mode at 1667 cm^{-1} (Figure 2c), as will be discussed further below. This phase contrast

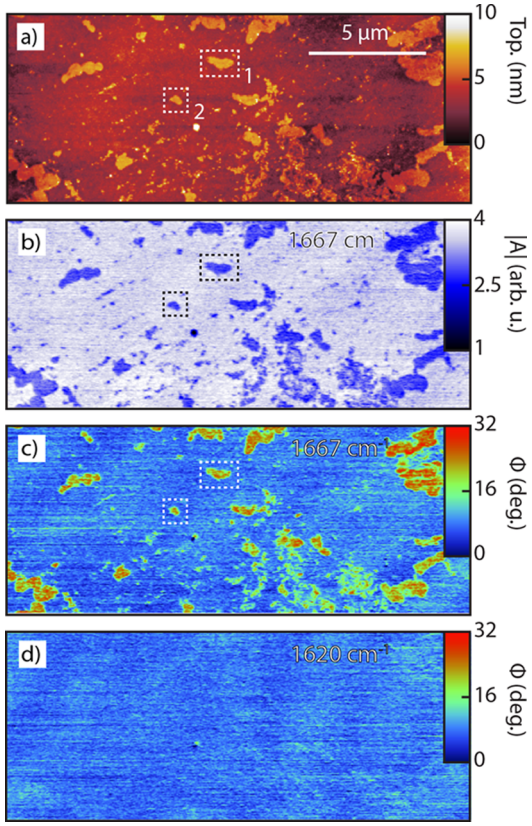

Figure 2. Large area scan with AFM topography (a), s-SNOM amplitude |A| (b) and phase ϕ with the excitation frequency on-resonance (c) and off-resonance (d) of the Amide I mode. Patches indicated by dashed rectangles (labeled 1 and 2) were chosen for subsequent spatio-spectral imaging measurements (see Figures 4 and S2).

disappears when the excitation frequency is detuned from resonance (to, e.g., 1620 cm^{-1}, as shown in Figure 2d).

For the subsequent detailed high-resolution spatio-spectral imaging, we select two representative bR regions (1 and 2) as indicated in Figure 2. Figure 3a shows a subset of such a spatio-spectral s-SNOM image sequence. This set of images demonstrates the evolution of phase contrast of membrane patch 1, acquired by tuning the optical frequency from $\bar{\nu}$ = 1580−1708 cm^{-1}. Figure 3b shows a s-SNOM phase spectrum $\phi(\bar{\nu})$ (circles, main panel) obtained from the full sequence of 26 scans at the location indicated by the dashed circle with signal averaged over a region with radius 50 nm. The signal is referenced against the gold surface with flat spectral phase ϕ_{Au}. The inset shows the corresponding normalized amplitude spectrum $|A(\bar{\nu})|$ (squares). The solid lines correspond to a fit of the imaginary and real parts of a Lorentzian, respectively, with peak position $\bar{\nu}_o$ = 1665 cm^{-1} and line width Γ = 34 cm^{-1}.

Peak position and line width of $\phi(\bar{\nu})$ correspond to resonance frequency and absorption line width and are in good agreement with previous IR absorption measurements of purple membrane.[12] This agreement is due to the near-field spectral phase $\phi(\bar{\nu})$ being approximately equal to the imaginary part of the s-SNOM amplitude $\mathrm{Im}(A(\bar{\nu}))$, which is, in turn, proportional to the imaginary part of the sample dielectric function $\phi(\bar{\nu}) \simeq \mathrm{Im}(A(\bar{\nu})) \propto \varepsilon_2 = 2nk$. This is a good approximation for weakly dispersive oscillators such as the Amide I mode.[9,11,24]

We examine patches 1 and 2 (Figure 2) more closely in order to probe the nanoscopic spatial protein composition of individual

dx.doi.org/10.1021/ja409815g | J. Am. Chem. Soc. 2013, 135, 18292−18295

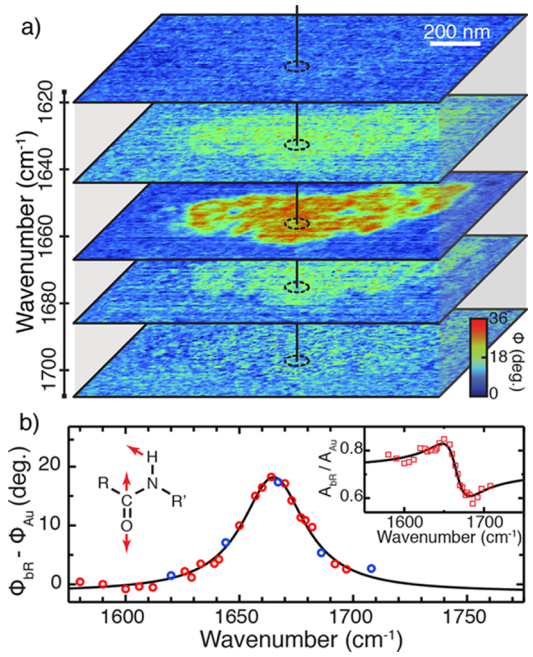

Figure 3. Spatio-spectral s-SNOM sequence of near-field phase images (a) acquired at incremental laser wavelengths showing the emergence and disappearance of IR-vibrational Amide I contrast. Local near-field phase spectrum (b) derived from the full sequence of 26 images at different wavelengths (circles) with fit to the imaginary part of a Lorentzian. Blue circles denote the scans shown in (a). Inset: Corresponding normalized amplitude spectrum (squares) with fit to the real part of a Lorentzian.

membrane patches. Figure 4 shows the tapping mode AFM topography (a) and corresponding s-SNOM phase and amplitude images (b and c) acquired under resonant Amide I excitation. Similar results are also found for patch 2, shown in Figure S2. The topography exhibits an average thickness of ∼5 nm, as expected. However, the topographic nonuniformity of up to ∼1 nm is larger than that seen for purple membrane on mica[21] and is in excess of the substrate roughness.

The s-SNOM phase image provides direct information on the local protein density. Similar to the topography, the s-SNOM phase image shows significant variation within the membrane patch. Shown in Figure 4d is a correlation plot of amplitude and phase versus topography for each pixel from the images (a−c). The amplitude exhibits the expected decrease in signal with increasing tip-Au separation. In contrast, the phase image shows three distinct regions corresponding to the Au substrate (Au), membrane with low protein concentration (mbr), and membrane with high protein concentration (bR). The inset shows the corresponding spatial location of each region. An overall lower topography and membrane protein concentration are seen at the edges, and a high protein concentration is seen within the membrane, in agreement with observations on mica.[25]

While the interior of the membrane shows an overall high protein concentration, a significant degree of morphological disorder is observed. Several defects in the patches with low topography and expected resulting low bR content can be made out, as specifically illustrated by a line cut taken along the dashed line in a and b (Figure 4e). These morphological defects are well reproduced in subsequent scans (Figure S1c) as further visualized in the correlation plot in Figure 4f. In addition to regions of correlation between low phase and low topography (i, iii, and v), clear anticorrelated regions exist as well, with either reduced thickness yet higher bR concentration (ii), or elevated topography and reduced bR concentration (iv).

This finding suggests the existence of regions with disordered membrane structure (with characteristic reduced topography being intrinsic or substrate roughness induced), with nonetheless contain high bR concentration. Similarly, regions of high membrane or accumulated impurity are observed with reduced bR concentration.[26] These results indicate a direct influence of the Au substrate on bR organization, resulting in a nonuniform

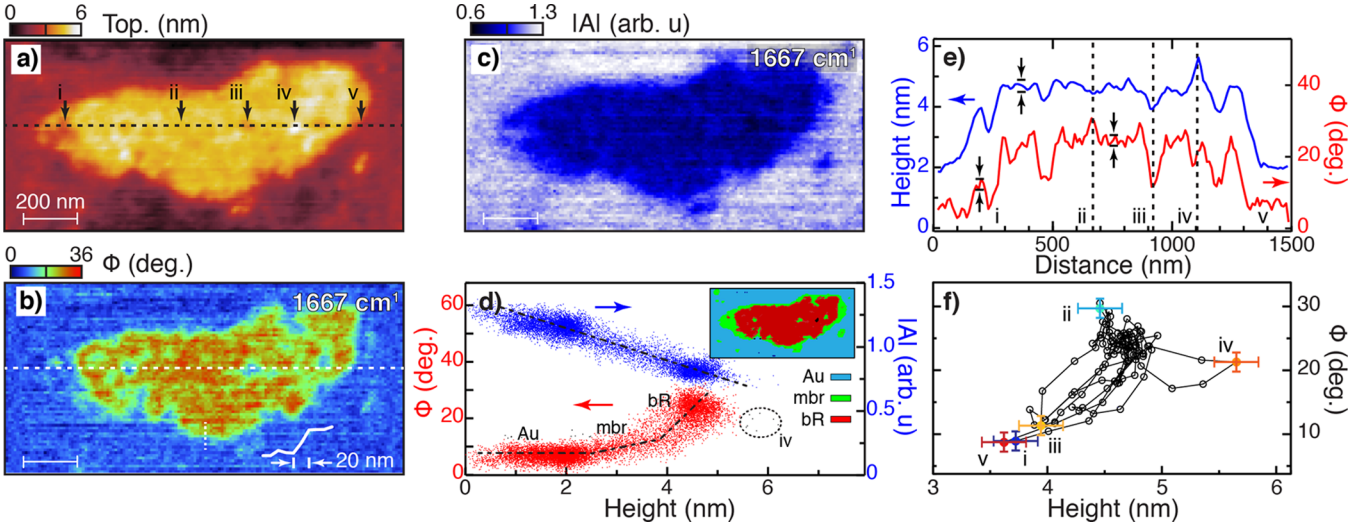

Figure 4. AFM topography (a), near-field phase image (b), and near-field amplitude image (c) of purple membrane patch 1 acquired under resonant excitation of the Amide I mode. The near-field phase and amplitude versus topography (d) show distinct regions of correlation between topography and phase arising from the Au substrate (Au), membrane with low protein concentration (mbr), and bR. Dashed lines are a guide to the eye. Corresponding map of the spatial location of each point (inset). Line trace (e) taken along the dashed lines in (a) and (b) with topography (blue) and phase (red), with points labeled as indicated (i−v, details see text), with corresponding correlation plot (f) of the same data shown in (e). Error bars in (f) and arrows in (e) indicate experimental uncertainty determined from RMS roughness across a homogeneous region in topography (±0.2 nm) and phase (±1.5°). Spatial resolution ≤20 nm is determined from line traces (e and vertical dotted line and inset in b).

dx.doi.org/10.1021/ja409815g | J. Am. Chem. Soc. 2013, 135, 18292−18295

membrane thickness that does not directly correlate with membrane protein concentration.

An analysis of our SNR suggests sensitivity approaching a few bR molecules. We make a conservative estimate of spatial resolution and sensitivity, assuming hexagonal close-packed bR arrangement of ideal purple membranes. Within our measured spatial resolution of ~20 nm and a bR trimer size of 5 nm,[27] the s-SNOM signal from the tip probes ~12 trimers with 253 amide groups per bR molecule.[28] The detected signal is the result of the interference between the near-field and reference field $S \propto \vec{E}_{nf} \cdot \vec{E}_{ref}$. Our noise σ is dominated by the reference arm laser noise and thus independent of near-field signal levels. With E_{ref} held constant, the SNR is related to the number of oscillators probed N_{osc} by $SNR \propto (E_{nf}/\sigma) \propto (N_{osc}/\sigma)$, with constant σ. With our measured SNR of ~15, this corresponds to 2−3 bR molecules detectable with SNR = 1. Additional increase in sensitivity may be possible through improved laser and interferometer stability, combined with increased signal averaging time as we demonstrated previously.[11]

The technique can be extended to biological structures containing different protein species with differing local environments and secondary structure. Structural variations and changes in the local environment result in variations in the spectral profile of the Amide I mode, which can be spatially mapped. Additional more broadly tunable sources could be used in imaging and separation of distinct protein species.

We use dried purple membranes on Au substrates to provide additional signal enhancement. However, IR s-SNOM is compatible with arbitrary surfaces and liquid environments. The expected signal decrease using dielectric substrates (e.g., atomically flat mica) can be compensated by longer measurement times provided by the use of an AFM with lower drift.[29] To extend s-SNOM to aqueous environments requires special design in order to minimize IR absorption in liquid and scattering or reflection at material interfaces. Further possibilities include the combination of s-SNOM with chemically sensitive time-domain techniques to probe molecular dynamics and interactions.[14,15]

Our results demonstrate the use of s-SNOM for the direct nanoimaging of protein concentration in purple membrane patches with few-protein sensitivity. The optical phase contrast, which emerges solely from the resonant excitation of the Amide I vibrational mode of the protein backbone complements conventional AFM topography with the chemical specificity inherent to vibrational nanospectroscopy. While demonstrated here for the case of purple membrane, this implementation can be extended to any biological structure exhibiting a suitable IR-active vibrational resonance.

■ ASSOCIATED CONTENT

Supporting Information

Experimental details and comparison between contact and tapping mode AFM on template stripped Au substrates. This information is available free of charge via the Internet at http://pubs.acs.org/

■ AUTHOR INFORMATION

Corresponding Author

markus.raschke@colorado.edu

Notes

The authors declare no competing financial interest.

■ ACKNOWLEDGMENTS

We thank Linda Randall for providing the halobacterium and protocols for preparing the bR sample, and Craig Prater from Anasys Instruments for technical scanning probe support. M.B.R. acknowledges support from the National Science Foundation (CHE-0748226). T.T.P. acknowledges support from the NSF (DBI-0923544, Phys-1125844) and NIST. T.T.P. is a staff member of the Quantum Physics Division of NIST. The Advanced Light Source is supported by the Director, Office of Science, Office of Basic Energy Sciences, of the U.S. Department of Energy under contract no. DE-AC02-05CH11231.

■ REFERENCES

(1) Scheuring, S.; Sturgis, J. N. *Science* **2005**, *309*, 484.
(2) Vaziri, A.; Tang, J.; Schroff, H.; Shank, C. V. *Proc. Natl. Acad. Sci* **2008**, *105*, 20221.
(3) Rust, M. J.; Bates, M.; Zhuang, X. *Nat. Meth.* **2006**, *3*, 793.
(4) Hell, S. W.; Wichmann, J. *Opt. Lett.* **1994**, *19*, 780.
(5) Novotny, L.; Stranick, S. J. *Annu. Rev. Phys. Chem.* **2006**, *57*, 303.
(6) Olmon, R. L.; Raschke, M. B. *Nanotechnology* **2012**, *23*, 444001.
(7) Deckert-Gauding, T.; Böhme, R.; Freier, E.; Sebesta, A.; Merkendorf, T.; Popp, J.; Gerwert, K.; Deckert, V. *J. Biophotonics* **2012**, *5*, 582.
(8) Yeo, B.-S.; Amstad, E.; Schmid, T.; Stadler, J.; Zenobi, R. *Small* **2009**, *5*, 952.
(9) Taubner, T.; Hillenbrand, R.; Keilmann, F. *Appl. Phys. Lett.* **2004**, *85*, 5064.
(10) Raschke, M. B.; Molina, L.; Elsaesser, T.; Kim, D. H.; Knoll, W.; Hinrichs, K. *ChemPhysChem* **2005**, *6*, 2197.
(11) Xu, X. G.; Rang, M.; Craig, I. M.; Raschke, M. B. *J. Phys. Chem. Lett.* **2012**, *3*, 1836.
(12) Rothschild, K. J.; Clark, N. A. *Biophys. J.* **1979**, *25*, 473.
(13) Diller, R.; Iannone, M.; Bogomolni, R.; Hochstrasser, R. M. *Biophys. J.* **1991**, *60*, 286.
(14) Hamm, P.; Zanni, M.*Concepts and Methods of 2D Infrared Spectroscopy*Cambridge University Press, 1998.
(15) Wang, L.; Middleton, C. T.; Zanni, M. T.; Skinner, J. L. *J. Phys. Chem. B* **2011**, *115*, 3713.
(16) Keilmann, F.; Hillenbrand, R. *Philos. Trans. R. Soc. London, Ser. A* **2004**, *362*, 787−805.
(17) Aubert, S.; Bruyant, A.; Blaize, S.; Bachelot, R.; Lerondel, G.; Hudlet, S.; Royer, P. *J. Opt. Soc. Am. B* **2003**, *20*, 2117.
(18) Taubner, T.; Keilmann, F.; Hillenbrand, R. *Nano Lett.* **2004**, *4*, 1669.
(19) Ocelic, N.; Huber, A.; Hillenbrand, R. *Appl. Phys. Lett.* **2006**, *89*, 101124.
(20) Butt, H.-J.; Downing, K. H.; Hansma, P. K. *Biophys. J.* **1990**, *58*, 1473.
(21) Müller, D. J.; Schabert, F. A.; Büldt, G.; Engel, A. *Biophys. J.* **1995**, *68*, 1681.
(22) Sullan, R. M. A.; Churnside, A. B.; Nguyen, D. M.; Bull, M. S.; Perkins, T. T. *Methods* **2013**, *60*, 131.
(23) Aizpurua, J.; Taubner, T.; García de Abajo, F. J.; Brehm, M.; Hillenbrand, R. *Opt. Expr.* **2008**, *16*, 1529.
(24) Govyadinov, A. A.; Amenabar, I.; Huth, F.; Carney, P. S.; Hillenbrand, R. *J. Phys. Chem. Lett.* **2013**, *4*, 1526−1531.
(25) Voitchovsky, K.; Contera, S. A.; Kamahira, M.; Watts, A.; Ryan, J. F. *Biophys. J.* **2006**, *90*, 2075.
(26) Near-field signal changes with tip−sample distance over the topographic variations in membrane thickness of $\lesssim$1 nm are negligible and thus do not induce topographic artifacts.
(27) Müller, D.; Engel, A. *Nat. Protoc.* **2007**, *2*, 2191.
(28) Khorana, H. G.; Gerber, G. E.; Herlihy, W. C.; Gray, C. P.; Anderegg, R. J.; Nihe, K.; Biemann, K. *Proc. Natl. Acad. Sci. U.S.A.* **1979**, *76*, 5046.
(29) King, G. M.; Carter, A. R.; Churnside, A. B.; Eberle, L. S.; Perkins, T. T. *Nano Lett.* **2009**, *9*, 1451.